chemosensors

MDPI

Article

Ppb-Level NO_2 Sensor with High Selectivity Fabricated by Flower-like Au-Loaded In_2O_3

Ji Zhang [1], Fangfang Zhang [1], Xu Li [2,*] and Qingji Wang [1,*]

[1] State Key Laboratory of Marine Resource Utilization in South China Sea, College of Information and Communication Engineering, Hainan University, Haikou 570228, China
[2] School of Chemical Engineering & Light Industry, Guangdong University of Technology, Guangzhou 510006, China
* Correspondence: lixu@gdut.edu.cn (X.L.); wangqingji@hainanu.edu.cn (Q.W.)

Abstract: With increasingly serious environmental problems caused by the improvement in people's living standards, the number of cars has increased sharply in recent years, which directly leads to the continuous increase in the concentration of NO_2 in the air. NO_2 is a common toxic and irritant gas, which is harmful to both the human body and the environment. Therefore, this research focuses on NO_2 detection and is committed to developing high-performance, low detection limit NO_2 sensors. In this study, flower-like Au-loaded In_2O_3 was successfully fabricated using the hydrothermal method and the wet impregnation method. The morphological features and chemical compositions of the as-prepared samples were characterized using SEM, TEM, XRD and XPS. A variety of sensors were fabricated and the gas-sensing properties of sensors were investigated. The results indicate that the sensor based on 0.5 mol% Au/In_2O_3 shows a response value of 1624 to 1 ppm NO_2 at 100 °C, which is 14 times that based on pure In_2O_3. Meanwhile, the detection limit of the sensor based on 0.5 mol% Au/In_2O_3 for NO_2 is 10 ppb, and the response value is 10.4. In addition, the sensor based on 0.5 mol% Au/In_2O_3 also has high selectivity to NO_2 among CO, CO_2, H_2, CH_4, NH_3, SO_2 and H_2S. Finally, the sensitization mechanism of Au/In_2O_3 was discussed, and the reasons for improving the performance of the sensor were analyzed. The above results and analysis demonstrate that the gas-sensing attributes of the sensor based on 0.5 mol% Au/In_2O_3 to NO_2 improved remarkably; at the same time, it has been proved that the composite material has extensive potential in practical applications.

Keywords: NO_2 sensor; *flower-like*; Au-loaded In_2O_3; low detection limit; high selectivity

check for updates

Citation: Zhang, J.; Zhang, F.; Li, X.; Wang, Q. Ppb-Level NO_2 Sensor with High Selectivity Fabricated by Flower-like Au-Loaded In_2O_3. *Chemosensors* **2023**, *11*, 289. https://doi.org/10.3390/chemosensors11050289

Academic Editor: Boris Lakard

Received: 28 March 2023
Revised: 1 May 2023
Accepted: 8 May 2023
Published: 12 May 2023

1. Introduction

With the rapid development of science and technology, the process of urbanization and industrialization has also accelerated. While bringing convenience to people's lives, the environmental pollution caused cannot be underestimated. On the one hand, the increase in car ownership directly leads to an increase in the content of NO_2 in the atmosphere; on the other hand, the exhaust gas emitted by factories is also one of the main sources of NO_2 [1–3]. As is known to all, NO_2 is a kind of common toxic and tangy gas, which is mainly generated from the emission of automobile exhaust and industrial waste gas. NO_2 is the main culprit of environmental problems such as acid rain and smog, which cause atmospheric pollution that affects the ecological balance of the planet [4–6]. Moreover, as long as the human body inhales 1 ppm of NO_2, it can cause lung disease and breathing difficulties, which seriously affect physical health [7]. Concurrently, the World Health Organization specifies that the standard value of NO_2, which is harmful to human health, is 40 μg/m^3 (~21.25 ppb) [8]. Therefore, how to detect NO_2 quickly and effectively has become one of the urgent problems to be solved. At present, commonly used gas detection methods in the market include mass spectrometry, chromatography and so on. Compared with these large-scale detection instruments, semiconductor gas sensors stand out in the field of gas detection because of their advantages of low cost, high performance, good portability

and easy integration [9–11]. However, with the improvement in people's environmental awareness, the technical requirements for gas sensors are higher than before, such as high response values, prominent selectivity and low detection limits. Thus, understanding how to develop NO_2 sensors with excellent sensing properties has attracted extensive attraction among researchers.

Up until now, among various semiconductor gas sensors, indium oxide (In_2O_3) is considered to be the most promising gas-sensing material due to its wide bandgap and high conductivity [12–15]. In recent years, it has been confirmed that In_2O_3 of different morphologies has great gas-sensing performances in NO_2 gas sensors, such as rod-shaped, sheet-shaped and flower-shaped [16]. According to reports, Shen et al. developed a NO_2 sensor with In_2O_3 nanorods using hydrothermal process, which has a response of 20.9 to 1 ppm NO_2 and a detection limit of 100 ppb (1.4) [17]. Yang et al. prepared a NO_2 sensor with In_2O_3 nanosheets via a hydrothermal process, and the sensor based on In_2O_3 nanosheets had a response value of 5.31 to 1 ppm NO_2 and a detection limit of 100 ppb (1.69) [7]. Zhou et al. fabricated a NO_2 sensor based on a In_2O_3 nanoflower using the hydrothermal method, which demonstrated a detection limit of 1 ppm NO_2 and a response of 2.1 [18]. In view of the above reports, it is not difficult to find that there are some defects regarding detection limits and response values because of the inherent properties of pure In_2O_3. In order to enhance the gas-sensing properties of the NO_2 sensor based on In_2O_3, people have attempted to load noble metal [19], construct heterojunctions [20] and compound conducting polymers [21], which have become research focuses in promoting gas-sensing properties. In the above properties-enhanced techniques, noble metal is not only used to provide high catalytic and high electroconductibility [22], but also to enhance adsorption ability for target gas on the surface of oxide, thus accelerating the electron transfer process between oxide and target gas [23–25]. In view of the above advantages, noble metal loading has proved to be one of the effective ways to improve sensor performance. Therefore, noble metal loading is used as the experimental method in this work to improve the performance of In_2O_3-based NO_2 sensors. In addition, the relevant literature and reports regarding In_2O_3-based sensors used to improve NO_2 performance through different strategies are summarized and listed, as shown in Table 1.

Table 1. The gas-sensing attributes of NO_2 sensor based on various In_2O_3.

Materials	Temp. (°C)	Conc. (ppm)	Response	DL (ppm)	Ref.
In_2O_3 microspheres	80	0.5	737.8	0.05	[26]
In_2O_3 microtubes	92	10	193	0.05	[27]
In_2O_3 nanowires	RT	5	740	0.01	[28]
In_2S_3/In_2O_3 nanoflower	160	10	251	2	[16]
Rb-doped flower-like In_2O_3	75	5	1502	0.1	[29]
In_2O_3 nanoparticles on GO	225	40	78	10	[30]
Au-loaded mesoporous In_2O_3	65	0.5	472.4	0.01	[24]
Flower-like 0.5 mol% Au/In_2O_3	100	1	1624	0.01	this work

Response: R_g/R_a; DL: detection limit.

In this work, various molar ratios of Au-loaded In_2O_3 (0 mol%, 0.3 mol%, 0.5 mol%, 1 mol%) were successfully fabricated via the hydrothermal method and the wet impregnation method. The morphological structure and chemical composition of samples prepared were characterized using XRD, SEM, TEM and XPS. Meanwhile, the as-prepared samples of different ratios were made into sensors, and gas-sensing performances were evaluated using a static test system. The results indicate that the sensors based on 0.5 mol% Au/In_2O_3 possess high response, excellent selectivity and a low detection limit toward NO_2. In addition, the gas-sensing mechanism was discussed by analyzing characterization and test results, which explained the reasons for improving the performance of sensors based on Au/In_2O_3. As such, it is demonstrated that this material has potential applications for NO_2 sensors and provides a reliable gas-sensitive material for NO_2 detection.

2. Experimental Section

2.1. Synthesis of Peach-Pit In_2O_3

In this experiment, all chemicals were purchased from Aladdin Reagent. All reagents were of analytical grade and used without further purification. Pure In_2O_3 was synthesized by a hydrothermal method. In a typical process, $InCl_3 \cdot 4H_2O$ (0.5 mmol) was dissolved in 15 mL of deionized water and then 15 mL of glycerol was successively added into the solution during gentle stirring until a homogenous solution was formed. Subsequently, trisodium citrate dihydrate $Na_3C_6H_5O_7 \cdot 2H_2O$ (1.75 mmol) was added into the above solution with vigorous stirring. When the mixed solution was stirred until homogeneity was reached, 250 μL of NaOH (0.1 M) was added into the solution and stirred to obtain a precursor solution. Finally, the precursor solution was transferred into a 50 mL PTFE-lined autoclave for hydrothermal process and heated at 190 °C for 16 h. After the autoclave was naturally cooled to room temperature, the samples were harvested by centrifugation with deionized water and absolute alcohol several times. Then, the samples were dried at 80 °C for 12 h and the white powders were collected. After that, the powders were transferred into a muffle furnace and annealed at 400 °C for 2 h with a heating rate of 2 °C/min to obtain peach-pit In_2O_3.

2.2. Synthesis of Flower-like Au-Loaded In_2O_3

Flower-like Au-loaded In_2O_3 was fabricated via the wet impregnation process. A total of 100 mg of the as-prepared peach-pit In_2O_3 was added into 10 mL of ethanol and processed by ultrasonic treatment for 20 min to obtain a uniformly dispersed solution. Subsequently, a suitable amount of $HAuCl_4 \cdot 3H_2O$ was added into the solution and stirred in a water bath at 40 °C until ethanol volatilized completely. After that, the precursor was collected and transferred into an Al_2O_3 boat. Then, the precursor was annealed at 300 °C for 2 h (2 °C/min) in a muffle furnace to obtain flower-like Au-loaded In_2O_3. Under the same experimental process, a series of Au-loaded In_2O_3 was successfully fabricated, and the molar ratios between Au and In_2O_3 were 0.3%, 0.5% and 1%.

2.3. Characterization of Samples

X-ray diffraction (XRD, Rigaku MiniFlex 600 X with Cu Kα1 radiation λ = 1.5406 Å) was used to obtain the crystal structure at 40 kV, 15 mA. A scanning electron microscope (PHENOM SCIENTIFIC ProX G5, Phenom, Rotterdam, Netherlands) was used to characterize the morphology and structure of the as-prepared samples. The detailed morphology of the as-prepared samples was characterized by transmission electron microscopy (FEI Tecnai G2 F30, FEI, Hillsboro, TX, USA). The chemical compositions of the as-prepared samples were obtained via X-ray photoelectron spectroscopy (Thermo escalab 250Xi, Thermo Fisher Scientific, Waltham, MA, USA).

2.4. Fabrication and Measurement of Gas Sensors

In this work, an Al_2O_3 ceramic tube structure (length: 4 mm, internal diameter: 0.8 mm, external diameter: 1.2 mm) was used. There was a pair of Au ring-shaped electrodes at each end of the Al_2O_3 ceramic tube with two Pt wires on each electrode as pins. The sensor was fabricated as follows: The as-prepared samples were mixed with deionized water to form a paste, which was then coated evenly onto the surface of the Al_2O_3 ceramic tube to form a sensing layer, and the tube was dried by infrared lamp for 15 min. Finally, the sensing device was annealed at 300 °C for 1 h with a heating rate of 2 °C/min to enhance the stability of the sensor. A sensor was used to insert a nickel chromium alloy wire into an aluminum oxide ceramic tube as a heater and weld it to a hexagonal base to obtain a sensor. The prepared device was aged for 24 h in a standard test environment for subsequent gas-sensitivity testing.

The gas-sensing performances were evaluated by a static test system (evaluation condition: 50% RH, 25 °C), where the heating current of the sensor was provided by a DC-regulated power supply, the resistance was recorded by multimeter and the data were

registered by computers. The response value of the NO_2 sensor is defined as R_g/R_a, where R_a is the resistance value of the sensor after stabilization after exposure to NO_2 and R_g is the resistance value of the sensor after stabilization in pure air. In addition, the response and recovery time of a sensor is defined as the time required for the resistance value of the sensor to reach 90% of the total resistance value change during the adsorption and desorption process.

3. Results and Discussion

3.1. Characterization of Material Structure

To investigate the crystal phase and purity of Au-loaded In_2O_3, the XRD of the as-prepared samples is shown in Figure 1. From the XRD images, the diffraction peaks of the as-prepared samples at 2θ angles of 22.37°, 30.99°, 32.61°, 45.61°, 50.25°, 57.20° and 58.19° can be observed, in which the diffraction peaks at the corners are consistent with the refractive indices of the crystal faces (012), (104), (110), (024), (116), (214) and (300), respectively. This corresponds to hexagonal In_2O_3 (JCPDS 22-0366). There are no diffraction peaks of other impurities observed in the XRD of Au-loaded In_2O_3, which can verify that the Au-loaded In_2O_3 composite had a certain high purity. The diffraction peaks of (006) and (113) crystal planes at angles of 37.2° and 37.7° gradually become wider peaks with the increase in Au content, which may be attributed to the (111) plane diffraction peak of Au NPs at an angle of 38.2° [31]. In addition, the other Au NPs diffraction peaks were not observed, probably due to the low content of Au [32]. The XRD results prove that the Au-loaded In_2O_3 samples were prepared successfully.

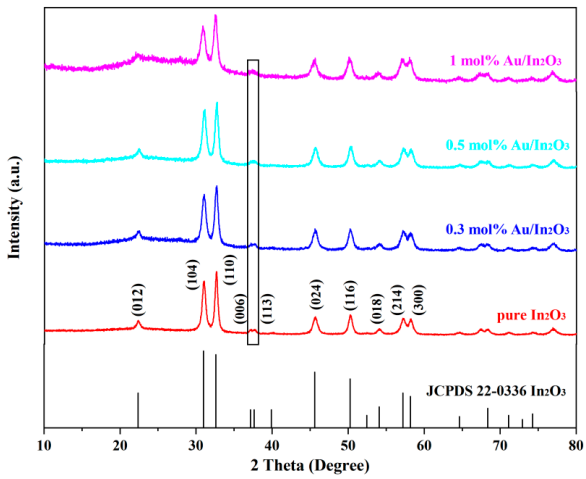

Figure 1. XRD spectra of the as-prepared samples.

Morphology and structure are two of the important factors affecting gas-sensing properties. The morphology and structure of peach-pit In_2O_3 and 0.5 mol% Au/In_2O_3 were characterized by SEM, as shown in Figure 2. It can be seen from Figure 2a,b that the diameter of peach-pit In_2O_3 was about 400 nm. Meanwhile, peach-pit In_2O_3 was identified to be pure phase because any other morphologies were not found in SEM. The morphological features of 0.5 mol% Au/In_2O_3 is shown in Figure 2c,d. Obviously, the morphology of 0.5 mol% Au/In_2O_3 became flower-like and its diameter was about 650 nm. Each flower was closely interwoven with nanosheets with a thickness of about 25 nm, constituting a flower-like uniform in size. At the same time, flower-like 0.5mol% Au/In_2O_3 was well dispersed without aggregation, and nanosheets are regularly stacked to form a flower-like structure. All the flowers bloomed, and the ultra-thin nanosheets were very loose, which provided rich space for gas diffusion. Through SEM images, it was found that the morphology and structure of Au/In_2O_3 changed, which can prove that gold-loaded Au/In_2O_3 was synthesized successfully.

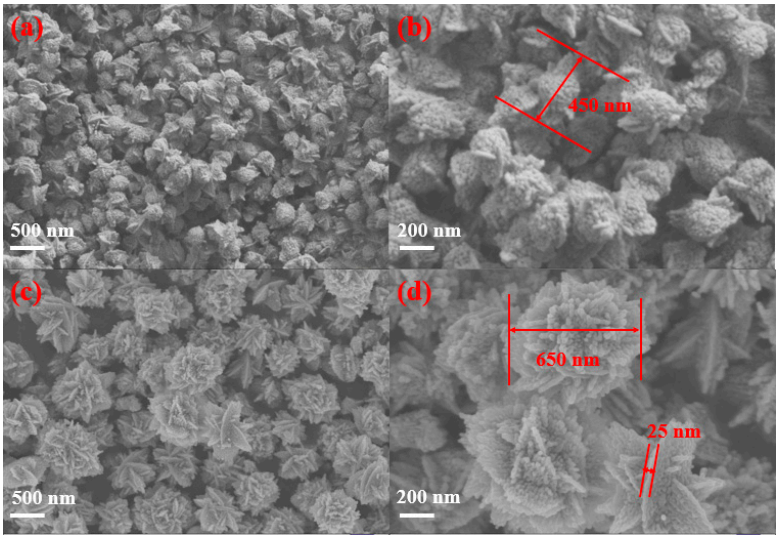

Figure 2. SEM images of peach-pit In_2O_3 (**a**,**b**) and 0.5 mol% Au/In_2O_3 (**c**,**d**).

Morphology details and crystal structures were characterized by TEM and HRTEM, as exhibited in Figure 3a–d. TEM images of 0.5 mol% Au/In_2O_3 are presented in Figure 3a,b, which show that the flower-like structure of 0.5 mol% Au/In_2O_3 has independent dispersion. HRTEM images of 0.5 mol% Au/In_2O_3 clearly show crystal lattice stripes in Figure 3c,d, which can prove that 0.5 mol% Au/In_2O_3 has high crystallinity. In addition, the lattice spacing of 0.28 nm and 0.27 nm was obtained from HRTEM images, which match with In_2O_3 (104) and (110) crystal planes, respectively. The lattice spacing of 0.14 nm corresponds to (111) planes of Au nanoparticles [33]. Additionally, In, Au and O elements are regularly dispersed from the element mapping images of 0.5 mol% Au/In_2O_3, as shown in Figure 3e–h. The elemental mapping of 0.5 mol% Au/In_2O_3 can further testify that Au-loaded In_2O_3 is developed successfully.

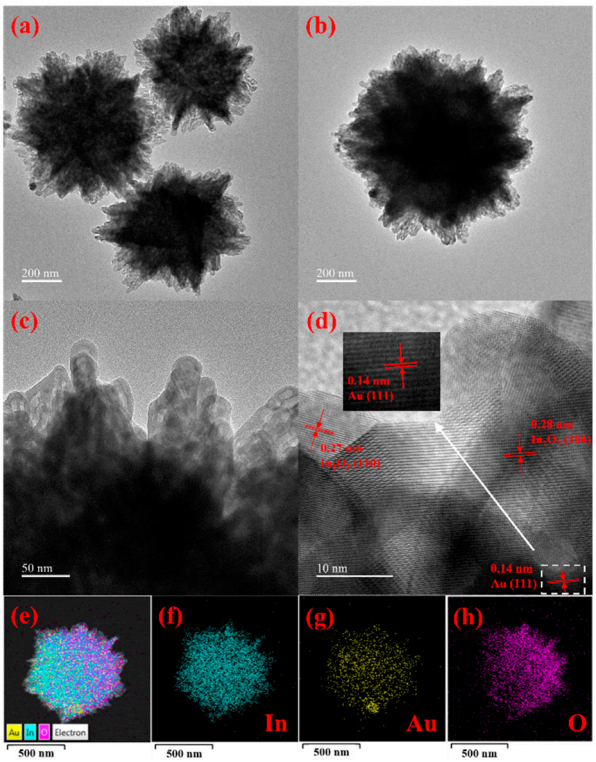

Figure 3. TEM and HRTEM (**a**–**d**) elemental mapping (**e**–**h**) of 0.5 mol% Au/In_2O_3.

The chemical compositions of In_2O_3 and 0.5 mol% Au/In_2O_3 were characterized by XPS, as shown in Figure 4a,b. The In 3d spectra of pure In_2O_3 and 0.5 mol% Au/In_2O_3 both presented two peaks at 444.0 eV, 451.6 eV and 444.1 eV, 451.7 eV, respectively, each of which is fitted to the In-O bond of In $3d_{5/2}$ and In $3d_{3/2}$ [34]. The O 1s spectra of In_2O_3 and 0.5 mol% Au/In_2O_3 are divided into three peaks by fitting process, as is exhibited in Figure 4b. The fitting peaks emerged at 529.5 eV, 531.2 eV, 532.1 eV and 529.6 eV, 531.2 eV 532.1 eV in pure In_2O_3 and 0.5 mol% Au/In_2O_3, which are assigned to lattice oxygen (OL), oxygen vacancy (OV) and chemical-adsorbed oxygen (OC), respectively [35]. Moreover, the content of oxygen species in pure In_2O_3 and 0.5 mol% Au/In_2O_3 are compared in Figure 4d, where the content of OL, OV and OC in pure In_2O_3 and Au/In-0.5 are 65.87%, 21.56%, 12.57% and 51.8%, 30.5%, 17.7%, respectively. Compared to pure In_2O_3, the contents of OV and OC in 0.5 mol% Au/In_2O_3 increased, which may be responsible for the improvement in gas-sensing properties. The Au 4f spectra of 0.5 mol% Au/In_2O_3 are shown in Figure 4c, where the peaks at 83.3 eV and 87.1 eV separately conform to Au $4f_{7/2}$ and Au $4f_{5/2}$ [36].

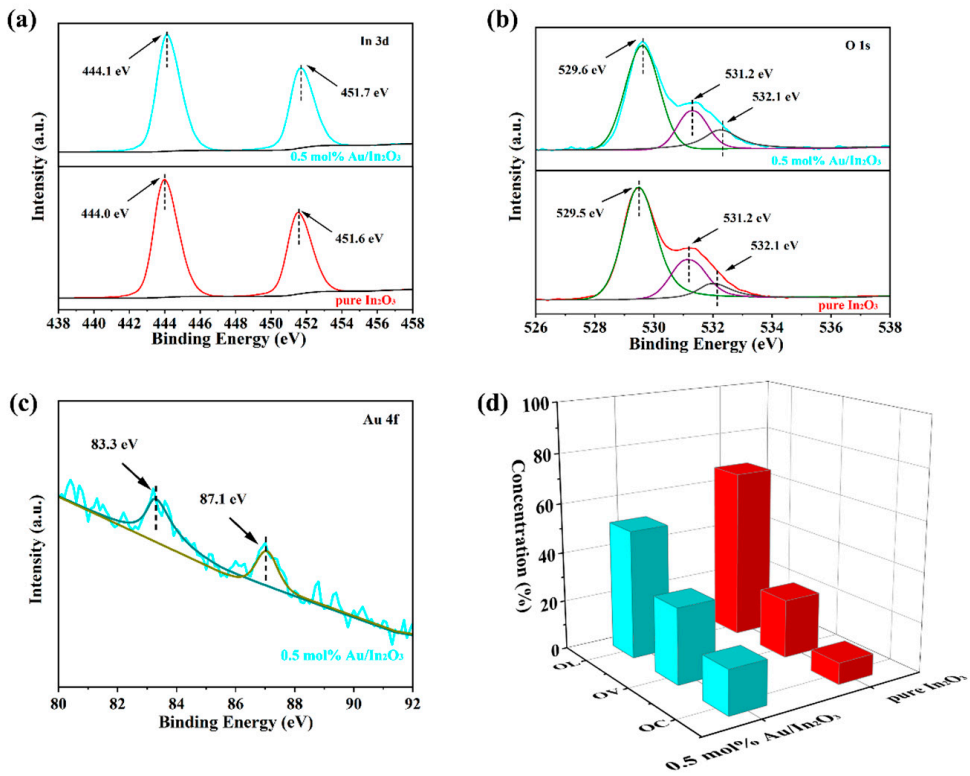

Figure 4. XPS spectrums of samples. The In 3d and O 1s of samples (**a**–**d**); the Au 4f of 0.5 mol% Au/In_2O_3 (**c**); oxygen species content of pure In_2O_3 and 0.5 mol% Au/In_2O_3 (**d**).

3.2. Gas-Sensing Properties

The operating temperature is the primary consideration for sensors, which is appraised by the response values of different sensors to 1 ppm NO_2 at different temperatures, as displayed in Figure 5a. It is apparent that the responses values of different gas sensors to 1 ppm NO_2 reach their maximum at 100 °C. The response values of sensors based on 0.5 mol% Au/In_2O_3 and pure In_2O_3 are1624 and 117 to 1 ppm NO_2 at 100 °C, respectively, and the response value of sensors based on 0.5 mol% Au/In_2O_3 is 14 times that of those based on pure In_2O_3. Therefore, 100 °C is regarded as the optimum operating temperature in this paper. The air resistance (R_a) of different sensors at different temperatures is exhibited in Figure 5b. Undoubtedly, R_a decreased as the temperature increased. Additionally, we found that the resistance of sensors based on different content of Au-loaded In_2O_3 was lower than that of pure In_2O_3 [25]. The transient curves of different sensors to 1 ppm NO_2 are exhibited in Figure 5c–f. The resistances of different sensors ascended in a NO_2

atmosphere, which conforms to the gas-sensing characteristics based on In_2O_3 sensors. Meanwhile, it is apparent that in NO_2, resistance changed drastically in the sensor based on 0.5 mol% Au/In_2O_3 compared to the other sensors, and that the gas-sensing attributes significantly improved.

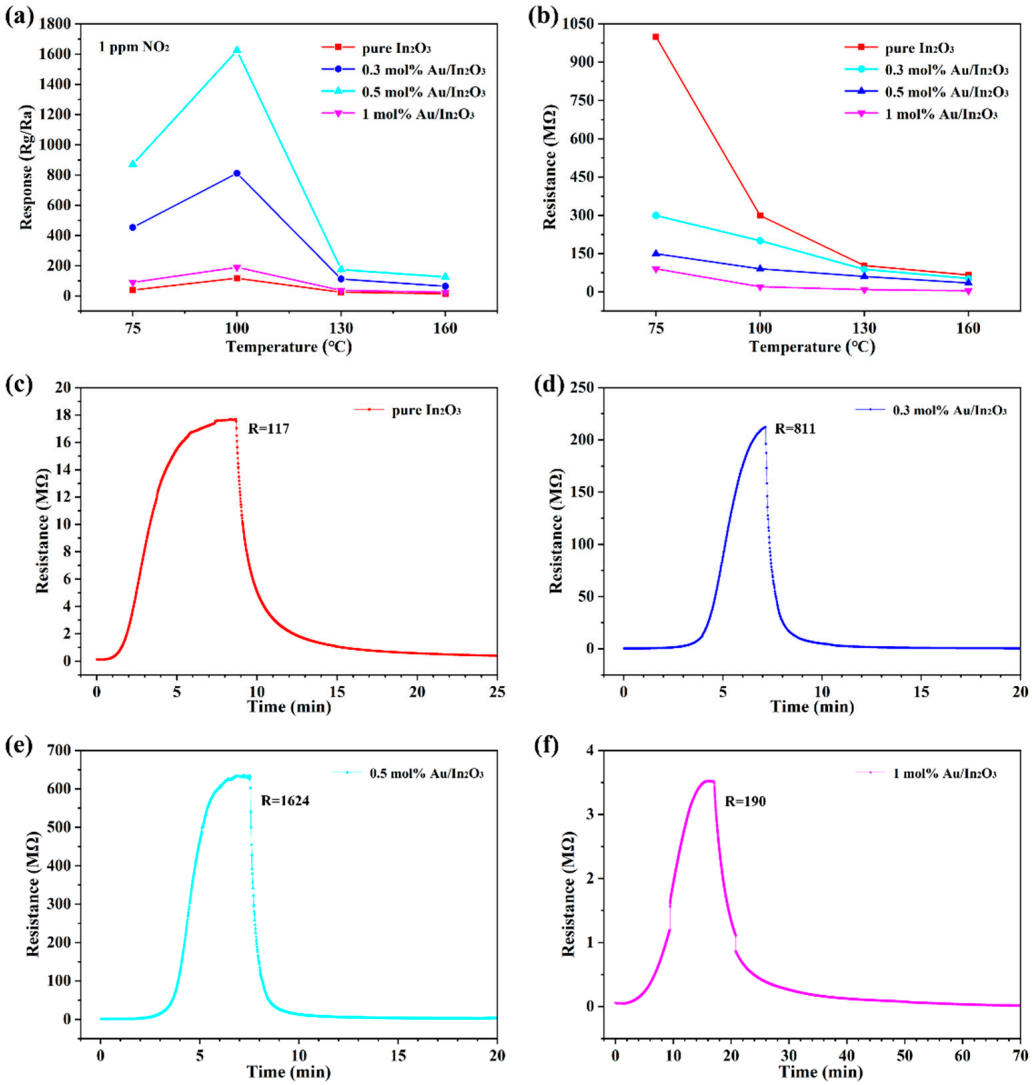

Figure 5. Response values and resistance values of different sensors at 75 °C to 160 °C (**a**,**b**); transient curve of different sensors at 100 °C (**c**–**f**).

The stability of the sensor represents the adaptability of the device to different concentrations of gas, while also reflecting the detection concentration range. Dynamic curves are used to further compare the gas-sensing properties of sensors based on 0.5 mol% Au/In_2O_3 and pure In_2O_3, as shown in Figure 6a,b. At different NO_2 concentrations, the gas-sensing properties of the sensor based on 0.5 mol% Au/In_2O_3 were promoted remarkably, in comparison with the sensor based on pure In_2O_3. Additionally, the response value greatly improved while the response recovery time did. Simultaneously, the detection limit of the sensor based on 0.5 mol% Au/In_2O_3 was boosted significantly. The detection limit of the sensor based on pure In_2O_3 was 50 ppb NO_2 and the response value was only 10. The detection limit of the sensor based on 0.5 mol% Au/In_2O_3 was 10 ppb NO_2 and had a response value of 10.4. Moreover, the response values of the sensor based on 0.5 mol% Au/In_2O_3 were positively correlated with increasing concentrations of NO_2, as displayed in Figure 6c. The transient response of the sensor based on 0.5 mol% Au/In_2O_3 to10 ppb NO_2 is shown in Figure 6d, where the response and recovery time is 390s and 270s, respectively.

To sum up, although low concentrations of NO_2, the sensor based on 0.5 mol% Au/In_2O_3 shows excellent gas-sensing properties. The above test and evaluation results prove that 0.5 mol% Au/In_2O_3 has good stability and a low detection limit, and that the detection range for NO_2 is very wide.

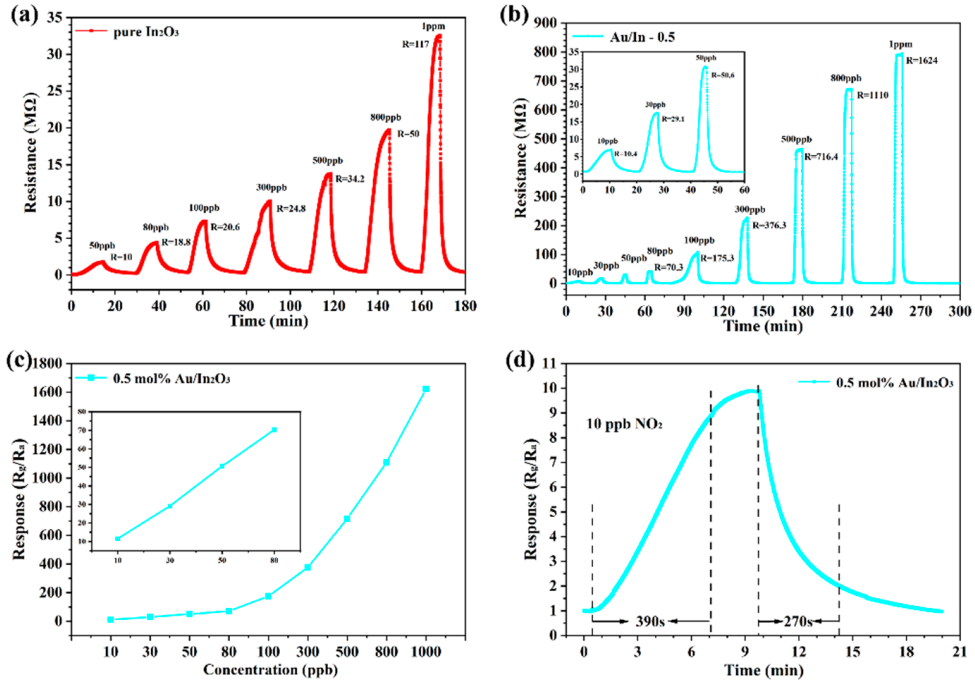

Figure 6. The dynamic response curve of sensors based on pure In_2O_3 and 0.5 mol% Au/In_2O_3 at 100 °C (**a**,**b**); response value of sensor based on 0.5 mol% Au/In_2O_3 (**c**); sensor based on 0.5 mol% Au/In_2O_3 vs. 10 ppb NO_2 transient curve (**d**).

Reproducibility and long-term stability jointly determine whether a sensor can be applied to practical indicators; these two performance parameters directly affect the service life and maintenance frequency of the sensor, which are very important in practical applications. The reproducibility of the sensor based on 0.5 mol% Au/In_2O_3 was evaluated in 500 ppb NO_2 five times, as is represented in Figure 7a. In the five-cycle experiment, the sensor based on 0.5 mol% Au/In_2O_3 was continuously and alternately exposed to 500 ppb NO_2 and air, which showed the settled response and recovery properties. Figure 7b signals the response values of the sensor based on 0.5 mol% Au/In_2O_3 to 500 ppb NO_2 in the five-cycle experiment, and it can be noticed that the response values did not change evidently throughout the five tests; meanwhile, the response characteristics were basically consistent. According to the above results, the sensor based on 0.5 mol% Au/In_2O_3 was provided with great reproducibility. The long-term stability of the sensor based on 0.5 mol% Au/In_2O_3 is exhibited in Figure 7c. The response values of the sensor based on 0.5 mol% Au/In_2O_3 at 500 ppb NO_2 presented no downward trend in 2 weeks and the variation was within 5%, which can prove that the sensor based on 0.5 mol% Au/In_2O_3 has good stability. Furthermore, the selectivity of the sensor based on 0.5 mol% Au/In_2O_3 is shown in Figure 7d, where the response values of the sensor based on 0.5 mol% Au/In_2O_3 to CO, CO_2, H_2, CH_4, NH_3 of 500 ppm, as well as SO_2 and H_2S of 10 ppm, were lower than that of 10 ppb NO_2. It is worth noting that the response value of the sensor based on 0.5 mol% Au/In_2O_3 of 10 ppb NO_2 was 6–10 times of that other interference gases ($R_{10\ ppb\ NO2}/R_{500\ ppm\ NH3} = 10$, $R_{10\ ppb\ NO2}/R_{10\ ppm\ H2S} = 6$), which shows that the sensor based on 0.5 mol% Au/In_2O_3 has bodacious selectivity to NO_2. In view of the test and evaluation results reproducibility, long-term stability and selectivity, it is shown that the sensor based on 0.5 mol% Au/In_2O_3 has certain practical application value. This article provides a new type of gas-sensing material for NO_2 sensors.

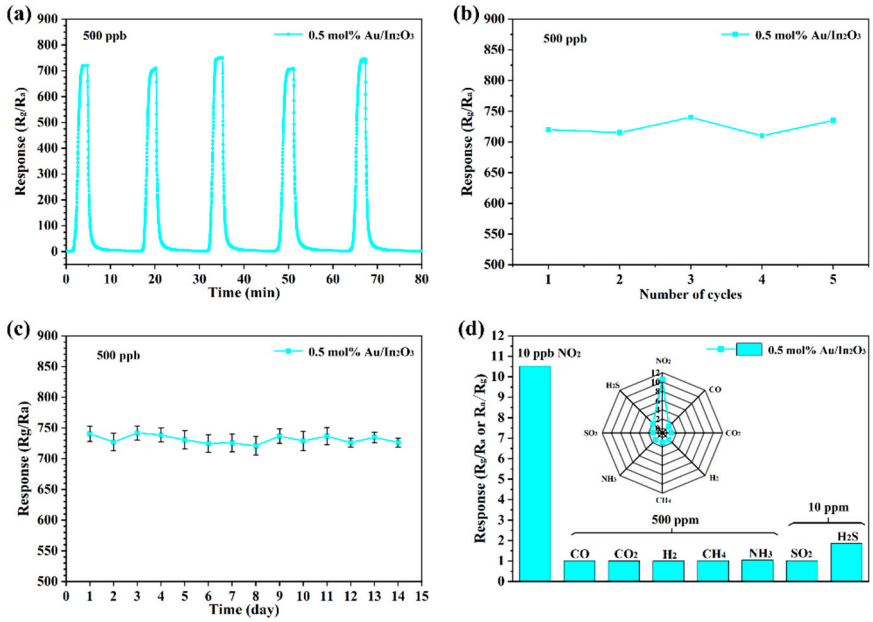

Figure 7. Five-cycle transient curve and its corresponding response values of sensor based on 0.5 mol% Au/In_2O_3 at 100 °C (**a**,**b**); long-term stability and selectivity (**c**,**d**).

3.3. Gas-Sensing Mechanism

The sensing mechanism of the sensor based on In_2O_3 is a process in which the target gas reacts with the adsorbed oxygen on the In_2O_3 surface to change the resistance [19]. In_2O_3 is a typical n-type semiconductor oxide, and when the sensor based on In_2O_3 is in the air, oxygen molecules combine with electrons in In_2O_3 to form active oxygen (O_2^-), as shown in Equations (1) and (2) [37]. When the sensor based on In_2O_3 makes contact with NO_2, the reaction is as follows: NO_2 not only reacts with the active oxygen on the surface of In_2O_3, but also occupies the electrons in the conduction band of In_2O_3. In short, NO_2 is paired with O_2^- and e^-, and the reaction is shown in Equations (3) and (4) [38,39]. When the sensor based on In_2O_3 is separated from NO_2, it returns to the initial state, as shown in Equation (5) [29].

$$O_2\ (gas) \rightarrow O_2\ (ads) \tag{1}$$

$$O_2\ (ads) + e^- \rightarrow O_2^-\ (ads) \tag{2}$$

$$NO_2\ (gas) + e^- \rightarrow NO_2^-\ (ads) \tag{3}$$

$$NO_2\ (gas) + O_2^-\ (ads) + 2e^- \rightarrow NO_2^-\ (ads) + 2O^-\ (ads) \tag{4}$$

$$NO_2^-\ (ads) + 2O^-\ (ads) \rightarrow NO_2\ (gas) + O_2\ (gas) + 3e^- \tag{5}$$

The reaction process of flower-like 0.5 mol% Au/In_2O_3 after contact with NO_2 is shown in Figure 8. The reasons for the remarkable improvement in gas-sensing performances based on 0.5 mol% Au/In_2O_3 can be attributed to the following three points: The first reason is that they can benefit from the specific morphology and structure. According to SEM and TEM images, the morphology of 0.5 mol% Au/In_2O_3 becomes a flower-like and is stacked by nanosheets. Moreover, flower-like 0.5 mol% Au/In_2O_3 has better dispersion than peach-pit In_2O_3, and there is no obvious aggregation of flower-like morphology and structure. The size of the small flowers is relatively uniform and well dispersed. In addition, abundant gaps are clearly displayed between adjacent nanosheets, which facilitates gas diffusion and enables sufficient reaction between the target gas and the sensing material. Therefore, dispersive and uniform morphology may provide a lot of space for the diffusion of gas molecules [39,40], which may promote gas-sensing performances; The second reason is due to the high catalytic activity of the noble metal Au. When In_2O_3-

based sensors come into contact with NO_2, they undergo an oxidation reaction on the surface of In_2O_3. Due to the inherent characteristics of In_2O_3 with insufficient surface activity, the reaction is not intense enough, resulting in poor gas-sensing performance. Owing to the high catalytic activity of Au, the activation energy of the chemical adsorption reaction of gas molecules can be reduced, and the chemical reaction rate can be increased. Accordingly, the gas-sensing performances of the sensor is enhanced [37]. The third reason can be attributed to the fact that 0.5 mol% Au/In_2O_3 has more OV and OC than pure In_2O_3. Based on the XPS characterization results, the content of OV and OC in 0.5 mol% Au/In_2O_3 is significantly higher than that in pure In_2O_3. The increase in OC content may make In_2O_3 have more reactive oxygen [38,41],which makes the oxidation reaction on the surface of In_2O_3 easier. As such, this may be another reason for improving gas-sensing performances. In consideration of the above three reasons, the performance of Au/In_2O_3-based sensors have been significantly improved, providing reliable gas-sensitive material for NO_2 detection.

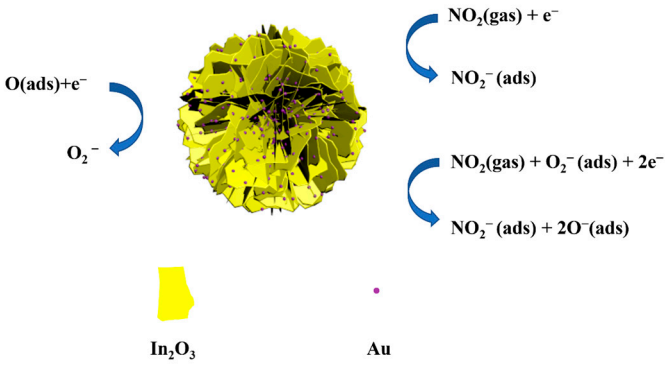

Figure 8. Diagram of gas-sensing mechanism of sensor based on 0.5 mol% Au/In_2O_3 to NO_2.

4. Conclusions

In summary, peach-pit In_2O_3 and flower-like 0.5 mol% Au/In_2O_3 were successfully prepared by the hydrothermal method and wet impregnation. The sensors based on different Au-loaded In_2O_3 were prepared for the evaluation of gas-sensing performances. Among those sensors, sensors based on 0.5 mol% Au/In_2O_3 exhibited excellent gas-sensitive properties. The specific performance is as follows: The response value of sensors based on 0.5 mol% Au/In_2O_3 is 1624 to 1 ppm NO_2 at 100 °C, which is 14 times higher than pure In_2O_3. Furthermore, the response value is 10.4 of sensors based on 0.5 mol% Au/In_2O_3 to 10 ppb NO_2, which can prove that this sensor has a low detection limit. The detection limit of the sensor based on pure In_2O_3 is 50 ppb, and the response value is only 10. In the meantime, the sensor based on 0.5 mol% Au/In_2O_3 also has good selectivity ($R_{10\ ppb\ NO2}/R_{500\ ppm\ NH3}$ = 10, $R_{10\ ppb\ NO2}/R_{10\ ppm\ H2S}$ = 6) and reliable repeatability. The sensitization mechanism is discussed through XRD, SEM, TEM, and XPS characterization analysis, and the improvement in the sensor based on 0.5 mol% Au/In_2O_3 performance can be attributed to the unique flower-like morphology, high catalytic activity of Au and the increase in oxygen species. The above reasons play a positive role in the diffusion and adsorption of NO_2 molecules for the sensor based on 0.5 mol% Au/In_2O_3. In conclusion, this work provides a new type of gas-sensing composite via a simple experimental method for NO_2 sensors and proves that this composite has potential application value.

Author Contributions: J.Z. and F.Z.: Writing—original draft; X.L.: Writing—review; Q.W.: Conceptualization and Supervision. All authors have read and agreed to the published version of the manuscript.

Funding: This work was funded by the National Nature Science Foundation of China (61803172), Hainan Provincial Natural Science Foundation of China (621RC509) and the Start-up Research Foundation of Hainan University (KYQD(ZR)1910).

Institutional Review Board Statement: Not applicable.

Informed Consent Statement: Not applicable.

Data Availability Statement: The data can be obtained from the corresponding author.

Acknowledgments: This work was funded by the National Nature Science Foundation of China (61803172), Hainan Provincial Natural Science Foundation of China (621RC509) and the Start-up Research Foundation of Hainan University (KYQD(ZR)1910).

Conflicts of Interest: The authors declare no conflict of interest.

References

1. Lin, H.; Wang, J.; Xu, S.; Zhang, Q.; Cheng, Y.; Han, D.; Wang, H.; Zhuo, K. Au-WO_3 Nanowire-Based Electrodes for NO_2 Sensing. *ACS Appl. Nano Mater.* **2022**, *5*, 14311–14319. [CrossRef]
2. Wang, Q.J.; Kou, X.Y.; Liu, C.; Zhao, L.J.; Lin, T.T.; Liu, F.M.; Yang, X.L.; Lin, J.; Lu, G.Y. Hydrothermal synthesis of hierarchical CoO/SnO_2 nanostructures for ethanol gas sensor. *J. Colloid Interface Sci.* **2018**, *513*, 760–766. [CrossRef] [PubMed]
3. Gu, D.; Liu, W.; Wang, J.; Yu, J.; Zhang, J.W.; Huang, B.Y.; Rumyantseva, M.N.; Li, X.G. Au Functionalized SnS_2 Nanosheets Based Chemiresistive NO_2 Sensors. *Chemosensors* **2022**, *10*, 165. [CrossRef]
4. Ahmadi, A.; Abbaspour, M.; Arjmandi, R.; Abedi, Z. Air Quality Risk Index (AQRI) and its application for a megacity. *Int. J. Environ. Sci. Technol.* **2015**, *12*, 3773–3780. [CrossRef]
5. Bai, M.J.; Chen, M.; Li, X.; Wang, Q.J. One-step CVD growth of ZnO nanorod/SnO_2 film heterojunction for NO_2 gas sensor. *Sens. Actuator B Chem.* **2022**, *373*, 132738. [CrossRef]
6. Bonyani, M.; Zebarjad, S.M.; Janghorban, K.; Kim, J.Y.; Kim, H.W.; Kim, S.S. Au-Decorated Polyaniline-ZnO Electrospun Composite Nanofiber Gas Sensors with Enhanced Response to NO_2 Gas. *Chemosensors* **2022**, *10*, 388. [CrossRef]
7. Yang, W.; Chen, H.; Lu, J. Assembly of stacked In_2O_3 nanosheets for detecting trace NO_2 with ultrahigh selectivity and promoted recovery. *Appl. Surf. Sci.* **2021**, *539*, 148217. [CrossRef]
8. Chowdhury, S.; Haines, A.; Klingmuller, K.; Kumar, V.; Pozzer, A.; Venkataraman, C.; Witt, C.; Lelieveld, J. Global and national assessment of the incidence of asthma in children and adolescents from major sources of ambient NO_2. *Environ. Res. Lett.* **2021**, *16*, 11. [CrossRef]
9. Wang, Q.; Wang, C.; Sun, H.; Sun, P.; Wang, Y.; Lin, J.; Lu, G. Microwave assisted synthesis of hierarchical Pd/SnO_2 nanostructures for CO gas sensor. *Sens. Actuators B Chem.* **2016**, *222*, 257–263. [CrossRef]
10. Wang, Q.J.; Bao, L.W.; Cao, Z.Q.; Li, C.Y.; Li, X.; Liu, F.M.; Sun, P.; Lu, G.Y. Microwave-assisted hydrothermal synthesis of Pt/SnO_2 gas sensor for CO detection. *Chin. Chem. Lett.* **2020**, *31*, 2029–2032. [CrossRef]
11. Meng, F.L.; Shi, X.; Yuan, Z.Y.; Ji, H.Y.; Qin, W.B.; Shen, Y.B.; Xing, C.Y. Detection of four alcohol homologue gases by ZnO gas sensor in dynamic interval temperature modulation mode. *Sens. Actuator B Chem.* **2022**, *350*, 130867. [CrossRef]
12. Tuerdi, A.; Yan, P.; He, F.G.; Abdukayum, A. Enhanced photocatalytic activity of a flower-like In_2O_3/$ZnGa_2O_4$:Cr heterojunction composite with long persisting luminescence. *RSC Adv.* **2022**, *12*, 34874–34881. [CrossRef] [PubMed]
13. Nasriddinov, A.; Tokarev, S.; Fedorova, O.; Bozhev, I.; Rumyantseva, M. In_2O_3 Based Hybrid Materials: Interplay between Microstructure, Photoelectrical and Light Activated NO_2 Sensor Properties. *Chemosensors* **2022**, *10*, 135. [CrossRef]
14. Ueda, T.; Boehme, I.; Hyodo, T.; Shimizu, Y.; Weimar, U.; Barsan, N. Enhanced NO_2-Sensing Properties of Au-Loaded Porous In_2O_3 Gas Sensors at Low Operating Temperatures. *Chemosensors* **2020**, *8*, 72. [CrossRef]
15. Meng, F.L.; Wang, H.; Yuan, Z.Y.; Zhang, R.Z.; Li, J. Ppb-Level Triethylamine Gas Sensors Based on Palladium Nanoparticles Modified Flower-Like In_2O_3 Grown on rGO Nanosheets Operating at Low Temperature. *IEEE Trans. Instrum. Meas.* **2022**, *71*, 1–9. [CrossRef]
16. Wang, B.-R.; Liu, L.-Y.; Guo, G.-C.; Bai, Y.-J.; Tu, J.-C.; Wang, R.-Z. Interface enhancement effect of hierarchical In_2S_3/In_2O_3 nanoflower heterostructures on NO_2 gas sensitivity. *Appl. Surf. Sci.* **2022**, *584*, 152669. [CrossRef]
17. Shen, Y.; Zhong, X.; Zhang, J.; Li, T.; Zhao, S.; Cui, B.; Wei, D.; Zhang, Y.; Wei, K. In-situ growth of mesoporous In_2O_3 nanorod arrays on a porous ceramic substrate for ppb-level NO_2 detection at room temperature. *Appl. Surf. Sci.* **2019**, *498*, 143873. [CrossRef]
18. Zhou, P.; Shen, Y.; Lu, W.; Zhao, S.; Li, T.; Zhong, X.; Cui, B.; Wei, D.; Zhang, Y. Highly selective NO_2 chemiresistive gas sensor based on hierarchical In_2O_3 microflowers grown on clinoptilolite substrates. *J. Alloys Compd.* **2020**, *828*, 154395. [CrossRef]
19. Liu, Y.; Li, S.; Xiao, S.; Du, K. In_2O_3 microtubes decorated with Ag nanoparticles for NO_2 gas detection at room temperature. *Vacuum* **2022**, *202*, 111197. [CrossRef]
20. Yuan, Z.-Y.; Yang, F.; Zhu, H.-M.; Meng, F.-L.; Ibrahim, M. High-response n-butanol gas sensor based on ZnO/In_2O_3 heterostructure. *Rare Met.* **2022**, *42*, 198–209. [CrossRef]
21. Han, C.; Li, X.; Liu, J.; Dong, H.; Cheng, W.; Liu, Y.; Xin, J.; Li, X.; Shao, C.; Liu, Y. In_2O_3/g-C_3N_4/Au ternary heterojunction-integrated surface plasmonic and charge-separated effects for room-temperature ultrasensitive NO_2 detection. *Sens. Actuators B Chem.* **2022**, *371*, 132448. [CrossRef]
22. Fan, Y.-Y.; Tu, H.-L.; Pang, Y.; Wei, F.; Zhao, H.-B.; Yang, Y.; Ren, T.-L. Au-decorated porous structure graphene with enhanced sensing performance for low-concentration NO_2 detection. *Rare Met.* **2020**, *39*, 651–658. [CrossRef]

23. Ding, M.D.; Xie, N.; Wang, C.; Kou, X.Y.; Zhang, H.; Guo, L.L.; Sun, Y.F.; Chuai, X.H.; Gao, Y.; Liu, F.M.; et al. Enhanced NO_2 gas sensing properties by Ag-doped hollow urchin-like In_2O_3 hierarchical nanostructures. *Sens. Actuator B Chem.* **2017**, *252*, 418–427. [CrossRef]
24. Li, S.; Cheng, M.; Liu, G.; Zhao, L.; Zhang, B.; Gao, Y.; Lu, H.; Wang, H.; Zhao, J.; Liu, F.; et al. High-response and low-temperature nitrogen dioxide gas sensor based on gold-loaded mesoporous indium trioxide. *J. Colloid Interface Sci.* **2018**, *524*, 368–378. [CrossRef]
25. Ueda, T.; Boehme, I.; Hyodo, T.; Shimizu, Y.; Weimar, U.; Barsan, N. Effects of Gas Adsorption Properties of an Au-Loaded Porous In_2O_3 Sensor on NO_2-Sensing Properties. *ACS Sens.* **2021**, *6*, 4019–4028. [CrossRef] [PubMed]
26. Hu, X.L.; Zhou, X.; Wang, B.; Sun, P.; Li, X.W.; Wang, C.; Liu, J.Y.; Lu, G.Y. Facile synthesis of hollow In_2O_3 microspheres and their gas sensing performances. *Rsc Adv.* **2015**, *5*, 4609–4614. [CrossRef]
27. Wang, N.; Ye, J.-X.; Sun, J.-B.; Zhang, X.-F.; Deng, Z.-P.; Xu, Y.-M.; Huo, L.-H.; Gao, S. Rapid and accurate detection of highly toxic NO_2 gas based on catkins biomass-derived porous In_2O_3 microtubes at low temperature. *Sens. Actuator B Chem.* **2022**, *361*, 131692. [CrossRef]
28. Zhang, B.; Bao, N.; Wang, T.; Xu, Y.; Dong, Y.; Ni, Y.; Yu, P.; Wei, Q.; Wang, J.; Guo, L.; et al. High-performance room temperature NO_2 gas sensor based on visible light irradiated In_2O_3 nanowires. *J. Alloys Compd.* **2021**, *867*, 159076. [CrossRef]
29. Wang, Y.; Yao, L.; Xu, L.; Wu, W.; Lin, W.; Zheng, C.; Feng, Y.; Gao, X. Enhanced NO_2 gas sensing properties based on Rb-doped hierarchical flower-like In_2O_3 microspheres at low temperature. *Sens. Actuator B Chem.* **2021**, *332*, 129497. [CrossRef]
30. Shah, S.; Han, S.; Hussain, S.; Liu, G.; Shi, T.; Shaheen, A.; Xu, Z.; Wang, M.; Qiao, G. NO_2 gas sensing responses of In_2O_3 nanoparticles decorated on GO nanosheets. *Ceram. Int.* **2022**, *48*, 12291–12298. [CrossRef]
31. Li, Z.; Zhang, Y.; Zhang, H.; Yi, J.X. MOF-derived Au-loaded Co_3O_4 porous hollow nanocages for acetone detection. *Sens. Actuator B Chem.* **2021**, *344*, 9. [CrossRef]
32. Lv, X.H.; Lan, H.; Guo, J.; Guo, M.X.; Yan, Y. Synthesis of Au-loaded $AgInS_2$ nanoparticles with highly enhanced visible light photocatalytic performances. *J. Mater. Sci.-Mater. Electron.* **2020**, *31*, 22284–22296. [CrossRef]
33. Ponnuvelu, D.V.; Dhakshinamoorthy, J.; Prasad, A.K.; Dhara, S.; Kamruddin, M.; Pullithadathil, B. Geometrically Controlled Au-Decorated ZnO Heterojunction Nanostructures for NO_2 Detection. *ACS Appl. Nano Mater.* **2020**, *3*, 5898–5909. [CrossRef]
34. Yu, Q.; Jin, R.; Zhao, L.; Wang, T.; Liu, F.; Yan, X.; Wang, C.; Sun, P.; Lu, G. MOF-Derived Mesoporous and Hierarchical Hollow-Structured In_2O_3-NiO Composites for Enhanced Triethylamine Sensing. *ACS Sens.* **2021**, *6*, 3451–3461. [CrossRef]
35. Liu, Y.; Liu, J.; Pan, Q.; Pan, K.; Zhang, G. Metal-organic framework (MOF) derived In_2O_3 and g-C_3N_4 composite for superior NOx gas-sensing performance at room temperature. *Sens. Actuator B Chem.* **2022**, *352*, 131001. [CrossRef]
36. Yang, G.; Ding, H.; Chen, D.M.; Feng, J.J.; Hao, Q.; Zhu, Y.F. Construction of urchin-like $ZnIn_2S_4$-Au-TiO_2 heterostructure with enhanced activity for photocatalytic hydrogen evolution. *Appl. Catal. B Environ.* **2018**, *234*, 260–267. [CrossRef]
37. Zhu, Q.; Gu, D.; Liu, Z.; Huang, B.; Li, X. Au-modified 3D SnS_2 nano-flowers for low-temperature NO_2 sensors. *Sens. Actuator B Chem.* **2021**, *349*, 130775. [CrossRef]
38. Kou, X.Y.; Wang, C.; Ding, M.D.; Feng, C.H.; Li, X.; Ma, J.; Zhang, H.; Sun, Y.F.; Lu, G.Y. Synthesis of Co-doped SnO_2 nanofibers and their enhanced gas-sensing properties. *Sens. Actuator B Chem.* **2016**, *236*, 425–432. [CrossRef]
39. Han, D.; Zhai, L.; Gu, F.; Wang, Z. Highly sensitive NO_2 gas sensor of ppb-level detection based on In_2O_3 nanobricks at low temperature. *Sens. Actuator B Chem.* **2018**, *262*, 655–663. [CrossRef]
40. Fan, F.Y.; Tang, P.G.; Wang, Y.Y.; Feng, Y.J.; Chen, A.F.; Luo, R.X.; Li, D.Q. Facile synthesis and gas sensing properties of tubular hierarchical ZnO self-assembled by porous nanosheets. *Sens. Actuator B Chem.* **2015**, *215*, 231–240. [CrossRef]
41. Wang, Z.H.; Hou, C.L.; De, Q.M.; Gu, F.B.; Han, D.M. One-Step Synthesis of Co-Doped In_2O_3 Nanorods for High Response of Formaldehyde Sensor at Low Temperature. *ACS Sens.* **2018**, *3*, 468–475. [CrossRef] [PubMed]